CRYSTAL GROWTH & DESIGN

Article

Cite This: *Cryst. Growth Des.* 2018, 18, 6995−7005

pubs.acs.org/crystal

Polymorphism, Crystal Packing, Twinning, and Molecular Conformations in 5′-Halo-5′-deoxyguanosines and a Hydrate of the Pseudohalide Analogue, 5′-Azido-5′-deoxyguanosine

Sean R. Parkin,*[,†] William H. Coldren,[‡] Joseph P. Fernandez,[‡] Christopher M. Hadad,[‡] and Edward J. Behrman[‡]

[†]Department of Chemistry, University of Kentucky, Lexington, Kentucky 40506, United States

[‡]Department of Chemistry and Biochemistry, Ohio State University, Columbus, Ohio 43210, United States

Supporting Information

ABSTRACT: Crystalline 5′-iodo-5′-deoxyguanosine (**I**) exists as a pair of solvent-free polymorphs (**Ia**, **Ib**) and as a mixed water/methanol solvate (**Ic**). The solvent-free polymorphs are capable of epitaxial intergrowth to give hybrid crystals that by visual inspection appear to be single crystals (Parkin et al. *Cryst. Growth Des.* **2016**, *16*, 6343−6352; hereafter PTGB). To investigate the generality and origin of the unusual polymorphism of the solvent-free forms, we have prepared and characterized the 5′-bromo- and 5′-chloro-5′-deoxyguanosine analogues (**II** and **III**, respectively), as well as the pseudohalide derivative 5′-azido-5′-deoxyguanosine (**IV**). Monoclinic and orthorhombic polymorphs of **II** (**IIa** and **IIb**, respectively) and an orthorhombic form of **III** all grow from water as small nonsolvated, tightly packed needles or laths. Although **IIa** is isostructural with the dominant polymorph of **I** (i.e., **Ia** in PTGB), all of these crystals (**IIa**, **IIb**, **III**) have similar molecular conformations and packing characteristics to **Ia**, in which the halogen adopts a *gauche* conformation relative to the deoxyribose ring oxygen. In spite of having different space group symmetries ($P2_1$ for **Ia** and **IIa** vs $P2_12_12_1$ for **IIb** and **III**), the crystal structures of **IIb** and **III** are also clearly related to **Ia**. Unlike **I**, however, no experimental evidence for conformational polymorphism, or of solvated forms was found for either **II** or **III**. Similar to PTGB work on **I**, density functional theory calculations show that the experimental *gauche* halide-atom conformations in **II** and **III** are ∼2.0 kcal/mol higher in energy than the energy-minimized *anti*-conformation (which occurs in the minor polymorph of **I**, i.e., **Ib**). The 5′-azido analogue (**IV**) in contrast, crystallized solely as a hydrate, initially forming minuscule irregular shards that were far too small for conventional X-ray analysis. By a process of Ostwald ripening, these shards could be enlarged sufficiently to allow structure determination by X-ray crystallography. The hydrate of **IV** shares many structural characteristics with **Ic**, but is much more complicated. It contains four independent molecules of **IV** (i.e., $Z' = 4$, vs $Z' = 2$ in **Ic**), which exhibit a range of distinctly different molecular conformations, as well as five full occupancy water molecules.

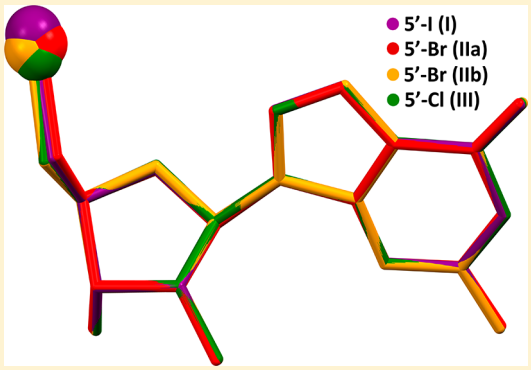

1. INTRODUCTION

5′-Iodo-5′-deoxyguanosine (**I**, Scheme 1) is a common starting material for the preparation of other 5′-substituted 5′-deoxyguanosines,[1] which are used for site-specific RNA modification.[2−4] Compound **I** crystallizes as a pair of conformational polymorphs (**Ia**, **Ib**) and as a mixed water/methanol solvate (**Ic**).[5] Although polymorphism, i.e., the phenomenon by which different crystal structures exist for identical chemical compositions, is common in molecular crystals,[6] **Ia** and **Ib** are unusual. Their constituent molecular conformations differ only by the torsion of the 5′-iodo substituent; packing of the 5′-deoxyguanosine moieties is virtually identical. Consequently, stacked layers in the two crystal forms are epitaxially compatible at interfaces where planes of deoxyguanosine moieties interact but not at contacts between planes of iodine atoms. Although not unknown in molecular crystals,[7−9]

Scheme 1. 5′-Substituted-5′-deoxyguanosines[a]

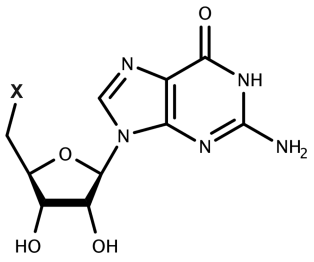

[a](**I**) X = I, (**II**) X = Br, (**III**) X = Cl, (**IV**) X = N_3.

Received: August 1, 2018
Revised: September 28, 2018
Published: October 8, 2018

DOI: 10.1021/acs.cgd.8b01162
Cryst. Growth Des. 2018, 18, 6995−7005

Table 1. Crystallographic Parameters for IIa, IIb, III, IV[a]

	Ia	IIa	IIb	III	IV
formula	$C_{10}H_{12}I_1N_5O_4$	$C_{10}H_{12}Br_1N_5O_4$	$C_{10}H_{12}Br_1N_5O_4$	$C_{10}H_{12}Cl_1N_5O_4$	$C_{10}H_{12}N_8O_4.5H_2O$
molecular weight	393.15	346.16	346.16	301.70	318.22[b]
temperature (K)	90.0(2)	90.0(2)	90.0(2)	90.0(2)	90.0(2)
crystal size (mm)	0.20 × 0.04 × 0.02	0.10 × 0.06 × 0.035	0.15 × 0.01 × 0.005	0.30 × 0.02 × 0.01	0.20 × 0.08 × 0.03
crystal system	monoclinic	monoclinic	orthorhombic	orthorhombic	monoclinic
space group	$P2_1$	$P2_1$	$P2_12_12_1$	$P2_12_12_1$	$P2_1$
a (Å)	7.6285(4)	7.5698(4)	5.0604(2)	5.0433(1)	9.2318(2)
b (Å)	4.9951(2)	4.9842(2)	7.5857(5)	7.5719(1)	27.0190(6)
c (Å)	17.1724(7)	15.8865(8)	31.4333(18)	30.8872(6)	10.8838(2)
β (deg)	91.843(2)	91.510(2)			93.254(1)
volume (Å^3)	615.95(5)	599.18(5)	1206.62(12)	1179.50(4)	2710.41(10)
density (Mgm^{-3})	2.120	1.919	1.906	1.699	1.621
Z, Z'	2, 1	2, 1	4, 1	4, 1	8, 4[c]
source, λ(Å)	Cu Kα, 1.54178	Mo Kα, 0.71073	Cu Kα, 1.54178	Cu Kα, 1.54178	Cu Kα, 1.54178
μ (mm^{-1})	6.686	3.455	4.902	3.129	1.148
total reflections	7526	15611	16928	10734	38874
unique reflections	1769	2758	2231	2387	10883
R_{int}	0.0379	0.0677	0.0789	0.0646	0.0362
R_1 [$I > 2\sigma(I)$]	0.0229	0.0339	0.0462	0.0497	0.0408
$wR_2(F^2)$ (all data)	0.0582	0.0604	0.1025	0.1250	0.1095
goodness-of-fit	1.062	1.050	1.170	1.119	1.044
Flack parameter[c]	0.019(9)	0.022(7)	−0.002(16)	−0.011(13)	0.05(5)
$\Delta\rho$ min/max (eÅ^{-3})	0.471/-0.851	0.366/-0.441	0.859/-0.681	0.484/-0.318	0.837/-0.316

[a]For ease of comparison, **Ia**, reproduced from PTGB[5] is also included. [b]5′-azido-5′-deoxyguanosine only, does not include the water molecules. [c]Absolute configurations known from the 5′-deoxyribose are clearly confirmed by the X-ray data.

2-D lattice compatibility is much more common in polytypic layered inorganic compounds, e.g., mica.[10] The term *allotwin*[11] was introduced to describe such well-defined mutual orientation of polytypes.

In the dominant polymorph of **I** (i.e., **Ia**), the torsion of the 5′-iodo substituent relative to the ring oxygen of the deoxyribose moiety is *gauche*, and ∼1.5 kcal/mol *higher* in energy than that of the minor polymorph, **Ib**, in which it is *anti*.[5] In a typical batch of freshly grown crystals of **I**, only a few percent of **Ib** was present. No single crystals of **Ib** were ever found; it was always intergrown with **Ia**, as in the aforementioned hybrid crystals. Moreover, on standing in mother liquor, **Ib** was found to gradually convert to **Ia** such that after ∼3 years no **Ib** could be detected. Given the torsional-energy advantage for the *anti* conformation in **Ib** over the *gauche* conformation in **Ia**, it is clear that the intermolecular environment within each polymorph must determine the overall stability of one polymorph relative to the other.

Intrigued by the possibility of similar hybrid-crystal growth in related 5′-deoxyguanosines, and to assess the effect of the 5′-substituent size, we initially focused on other halides, specifically 5′-bromo-5′-deoxyguanosine[12,13] (**II**) and 5′-chloro-5′-deoxyguanosine[14−17] (**III**). There being no conveniently available halogen larger than iodine, we broadened the scope to include pseudohalides, resulting in the azide derivative 5′-azido-5′-deoxyguanosine[18,19] (**IV**), a compound that has found use as a reagent for "click" chemistry in RNA work.[20−22] In spite of the fact that compounds **II**, **III**, and **IV** have been known for many years, their crystal structures have not been reported prior to this work. Other derivatives were also considered (including 5′-cyano and 5′-amino), but the reaction yields were very low and no suitable crystals could be obtained.

In this paper we describe the crystal structures and hydrogen bonding of solvent-free crystals of **II** and **III**, and with the aid of computational modeling, compare them to solvent-free **I**. The crystal structure of **IV**, a hydrate, turned out to be

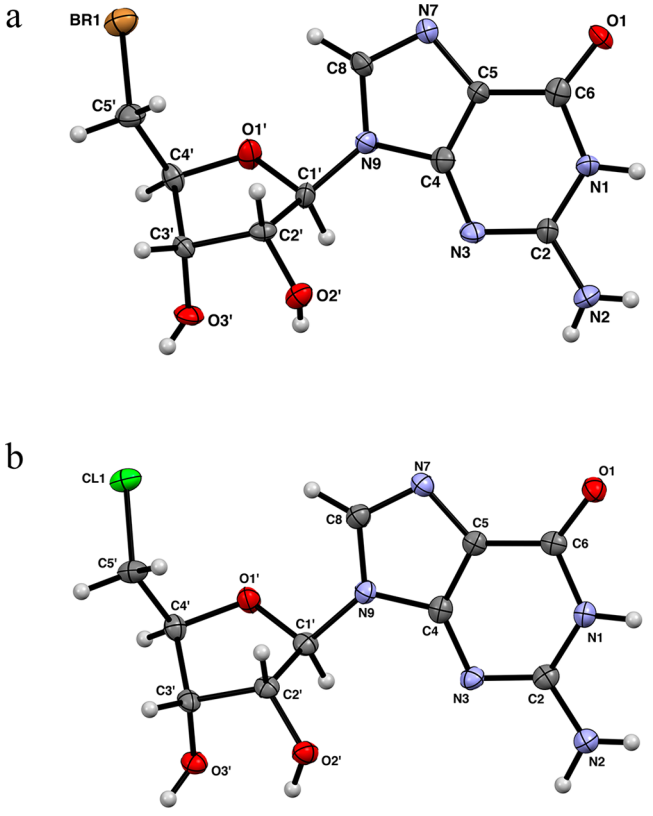

Figure 1. Ellipsoid plots (50% probability) of (a) structure **IIa** and (b) structure **III**. Atom connectivity and conformation in structure **IIb** is virtually indistinguishable from **IIa**, so is given in the Supporting Information (Figure S2).

DOI: 10.1021/acs.cgd.8b01162
Cryst. Growth Des. 2018, 18, 6995−7005

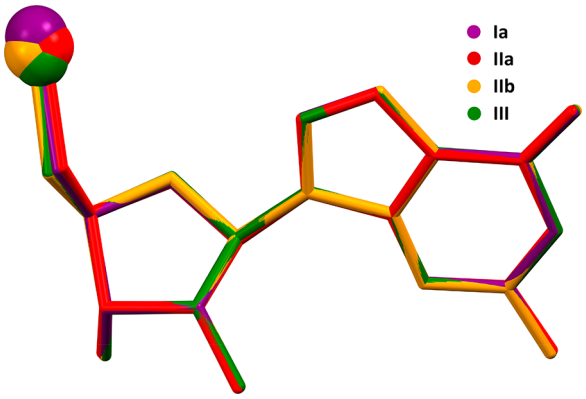

Figure 2. An overlay of 5′-X-5′-deoxyguanosines from a least-squares fit of 5′-deoxyguanosine moiety atoms for the crystal structures of (**I**) X = I, (**II**) X = Br, (**III**) X = Cl. Halogen atoms are drawn as balls for emphasis.

considerably more complicated than anticipated. It shares a number of similar features to **Ic**, the mixed water/methanol solvate of **I**. We therefore also describe its structure in detail, assess its similarities with **Ic**, and attempt, with the aid of computational modeling, to make sense of the varied molecular conformations adopted by the four main molecules in the asymmetric unit.

2. EXPERIMENTAL SECTION

2.1. Synthesis and Crystallization. *2.1.1. 5′-Bromo-5′-deoxyguanosine [CA: 1146729-83-0].* Previous reports of the synthesis of **II** gave no useful details.[12,13] Attempts to make it by the Appel reaction[23] from guanosine using many variations of the procedures described by Tsuji and Takenaka[24] failed; only guanosine could be recovered. Dean reported similar findings.[19] Compound **II** was synthesized in good yield by application of the Finkelstein reaction[25] to **I**[1,26] following the procedure described by Parker.[27] **I** (0.2 g, 0.51 mmol) and $[N(^nBu)_4]Br$ (0.4 g, 1.25 mmol) were dissolved in 4 mL *N*-methylpyrrolidinone (NMP) at room temperature (RT). After standing at RT overnight, the yellow solution was poured with stirring into 175 mL dichloromethane (DCM). The product (0.165 g, 90%) was filtered and washed. Some of the iodo starting material was still present so the procedure was repeated with 0.3 g $[N(^nBu)_4]Br$ and 3 mL NMP to yield 0.140 g of product. The sequential treatment is necessary because the product does not precipitate from DCM in the presence of a large excess of $[N(^nBu)_4]Br$. Crystallization was carried out by treating 50 mg of **II** with 4 mL of boiling water until almost all was dissolved. Crystals formed at RT upon slow cooling. These were washed with cold water and dried. Polymorphs **IIa** and **IIb** formed in separate batches under similar conditions, but no concomitant polymorphism was observed (see section 3.3, below). The NMR spectra of **II** in DMSO-d_6 are almost identical to those of **I** except for the two 5′-proton resonances at δ 3.79 and 3.67 ppm, and the 5′-carbon resonance at δ 33.86 ppm [the corresponding values for **I** are δ 3.56, 3.42, and 8.02 ppm]. Anal.: Calcd for $C_{10}H_{12}N_5O_4Br$: C, 34.7; H, 3.49; N, 20.2. Found: C, 34.8; H, 3.29; N, 20.0.

2.1.2. 5′-Chloro-5′-deoxyguanosine [CA: 21017-09-4]. Compound **III** has been well documented.[14−17] It was made here in a similar way to **II**. **I** was reacted with $[N(^nBu)_4]Cl$ identically to the procedure used for **II** but, in this case, only the first displacement step was required to react all of the iodo starting material. The precipitate obtained from addition of DCM was gelatinous and contained both NMP and $[N(^nBu)_4]Cl$. These were easily removed upon crystallization of 100 mg of the crude material from 7 mL of boiling water. Again, the NMR spectra differed from the iodo and bromo compounds only for the two 5′-proton resonances at δ 3.90 and 3.80 ppm and for the 5′-carbon resonance at δ 44.8 ppm.

2.1.3. 5′-Azido-5′-deoxyguanosine [CA: 42204-44-4]. The 5′-azido derivative[18,19] **IV** was made following Dean's procedures,[19] though reaction under argon was not required. Its proton and ^{13}C NMR spectra agreed with literature values.[19] Crystallization from 50 parts of water[18] yielded minuscule clusters of shards with typical dimensions ∼0.05 × 0.01 × 0.005 mm^3 that were far too small for home-laboratory X-ray crystallography. Ostwald ripening at 40 °C for ∼2 h grew these shards

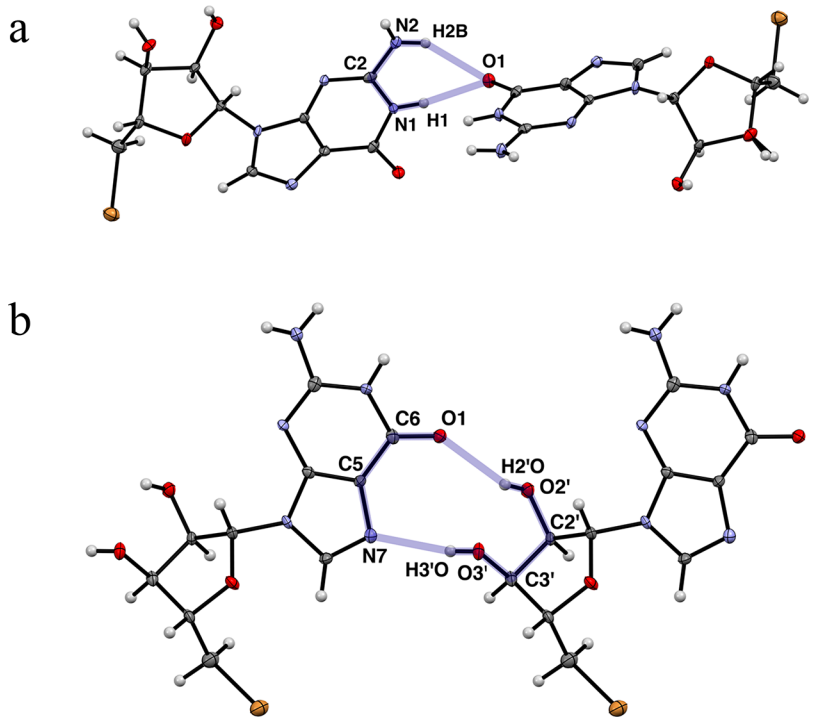

Figure 3. Main hydrogen-bonding motifs in **IIa**, **IIb**, and **III** (and **Ia** of PTGB), highlighted by thick semitransparent blue lines. (a) An $R^1_2(6)$ ring between 2_1 screw-related molecules, with bifurcated carbonyl oxygen acceptor. (b) An $R^2_2(10)$ ring formed by deoxyribose hydroxyl donors and purine carbonyl O and 5-membered ring N acceptors on a translation-related (diagonal in the *ab*-plane) molecule.

DOI: 10.1021/acs.cgd.8b01162
Cryst. Growth Des. 2018, 18, 6995−7005

Table 2. Conformation-Defining Torsion Angles and Deoxyribose Ring Puckering Parameters for IIa, IIb, III[a]

	Ia	IIa	IIb	III
C4−N9−C1′−O1′ (deg)	−152.4(5)	−152.1(4)	−153.3(7)	−153.4(4)
C8−N9−C1′−O1′ (deg)	28.5(7)	30.2(6)	24.1(10)	26.4(6)
O1′−C4′−C5′−X[a] (deg)	61.2(5)	61.6(5)	58.3(7)	54.6(4)
C3′−C4′−C5′−X[a] (deg)	178.8(4)	178.5(3)	175.1(5)	172.1(3)
Cremer-Pople Q (Å)	0.384(6)	0.384(5)	0.375(8)	0.375(8)
Cremer-Pople Φ (deg)	93.1(8)	95.2(7)	83.0(11)	83.8(7)

[a]Ia: X = iodine; IIa, IIb: X = bromine; III: X = chlorine. For comparison, parameters for Ia from PTGB[5] are included.

into semiregular laths large enough (typically ∼0.20 × 0.05 × 0.02 mm^3) to attempt structure determination by X-ray diffraction. On further standing for ∼1 year at RT, the largest single crystals had grown to over 0.5 mm in length; they indexed to give the same unit cell as hydrate **IV** (Table 1). Attempts to grow anhydrous crystals using DMF, DMSO, or ethylene glycol as cosolvents with methanol or ethanol, by vapor diffusion with benzene or methanol, from the melt, or by sublimation were unsuccessful.

2.2. Single-Crystal Data Collection. Similar to **I** in PTGB, all crystals obtained were small (Table 1, Figure S1). Crystals of **IIa** used for data collection were colorless laths, **IIb** and **III** were colorless needles, while that of **IV** was a colorless semiregular wedge-shaped lath. In each case, crystals were first submerged in polyisobutene oil,[28] cleaned of adhering debris, and mounted on either a fine glass fiber (**IIb**, **III**, **IV**) or a nylon loop (**IIa**) under a polarizing microscope. Crystals were mounted directly into a cold-N_2 stream angled relative to the ϕ axis[29] (CryoIndustries LT-2 or LT-3) and data were collected at 90.0(2) K using ϕ and ω scans with Cu Kα or Mo Kα (**IIa** only) X-rays on either a CCD-based rotating-anode Bruker-Nonius X8 Proteum (**IIb**) or a CMOS Bruker D8 Venture dual-microsource κ-axis diffractometer (**IIa**, **III**, **IV**), each equipped with multilayer focusing optics. Raw diffraction images were integrated using SaintPlus in either APEX2[30] (**IIb**) or APEX3[31] (**IIa**, **III**, **IV**). Data scaling, merging, and absorption correction used well-established procedures.[32,33] A summary of crystal and data collection parameters is given in Table 1.

2.3. Structure Solution and Refinement. Structures were solved using SHELXT[34] and refined using SHELXL.[35] Hydrogen atoms in all four structures were found in difference-Fourier maps. Hydrogens on the main 5′-deoxyguanosine molecules were included using riding models except for those of the exocyclic amine and hydroxyl groups, which were refined. In **IV**, the hydrogens of five water molecules were refined with geometry restraints. The largest residual electron density peak (0.84 e Å^{-3}) was quite large for a light-atom structure. When modeled as a partial water oxygen, its occupancy factor refined to about 0.2, but it was too close to hydroxyl oxygen O3′B (2.333 Å) and to a translation (x, y, z+1) related carbonyl O1B (2.383 Å). It could simply be a minor occupancy fragment of nonmodeled disorder, but there was no particular reason to suspect disorder of other nearby atoms. Since it made little difference to the overall refinement if it was ignored, included as partial water, or removed with SQUEEZE,[36] we chose to ignore it. For the riding models, standard low-temperature distances were applied [0.95 Å (Csp^2H), 0.99 Å (R_2CH_2), 1.00 Å (R_3CH), 0.88 Å (NH)]. In all cases, hydrogen atom U_{iso} values were tied to their parent atom U_{eq} values (1.5U_{eq} for NH_2, OH, and CH_3; 1.2U_{eq} for all others). Refinement progress was monitored using established procedures.[37−39] Refinement statistics are given in Table 1.

2.4. Powder Diffraction. Separate batches of **IIa**, **IIb**, **III**, and **IV** were ground using a small agate mortar and pestle. For each sample, the compressed powder was packed into a fine kapton tube (∼0.2 mm i.d.). Two-dimensional powder diffraction images were collected on the same Bruker D8 Venture diffractometer used for single-crystal studies. Data collection consisted of 360° rotation about the ϕ axis for 60 s or 180 s (**IV** only) at 90.0(2) K using Cu Kα X-rays. Images were radially integrated over a 2θ range of 1.3−50° with tools in APEX3.[31]

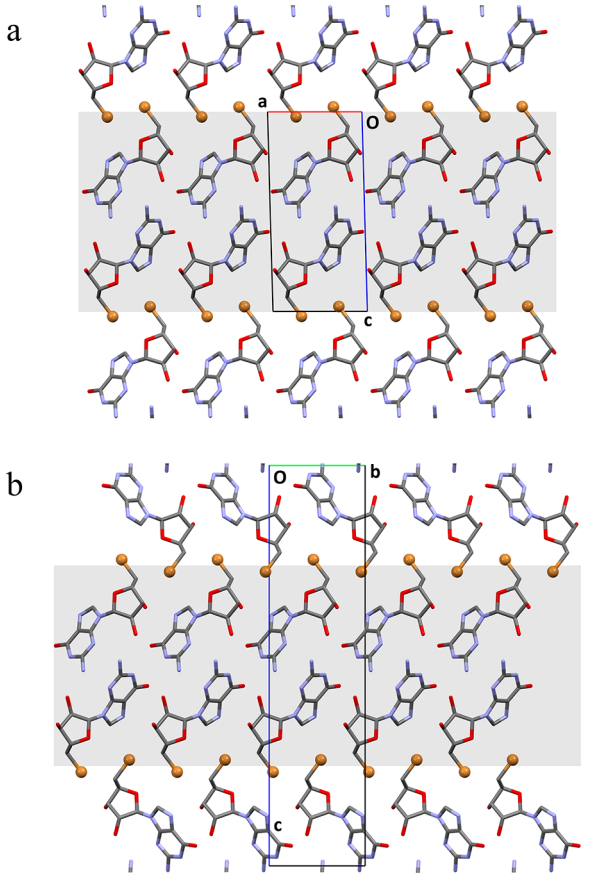

Figure 4. Alternation of double layers in (a) **IIa** viewed down its b-axis: the shaded double layer is identical to the unshaded layers above and below (translated along c); (b) **IIb** viewed down its a-axis: the shaded double layer is similar to the shaded double layer in **IIa**, but the unshaded layers above and below are 2_1 screw related (rotated about c by 180° and translated half a cell repeat along c). Bromine atoms are drawn as spheres for emphasis. Similar diagrams are given in the SI for **IIa** viewed down a and **IIb** viewed down b (Figure S3).

Simulated powder diffraction patterns based on the single-crystal structures of **II** and **III** were obtained using Mercury.[40] For ease of comparison, calculated powder peaks were broadened slightly to better approximate the width of the experimental powder diffraction peaks.

2.5. Computational Details. Density functional theory (DFT) calculations were performed with Gaussian 16 at the Ohio Supercomputer Center.[41] Geometries of **IIb** and **III** were optimized with the B3LYP functional, using the 6-31+G* basis set for nonhalogen atoms (C, H, O, N), while the larger 6-311+G* basis set was used for halogen atoms (Br, Cl).[42−45] Optimized structures were confirmed as local minima on the relevant potential energy surface by vibrational frequency analyses. Root-mean-square-deviation (RMSD) analyses between the crystal structures and geometry optimized structures were performed with the UCSF Chimera package.[46] At the same level of theory, a relaxed-coordinate dihedral scan was conducted on the O1′-C4′-C5′-X angle of the optimized structures over the full 360° in 15° increments. Results of the optimizations and scans were visualized with GaussView 6.[47] For the four independent main molecules in **IV**, geometry optimization and vibrational frequency analyses were conducted at the B3LYP/6-311+G** level of theory for both gas phase and solvated (SMD,[48] water) molecules.

3. RESULTS AND DISCUSSION

3.1. Structures of 5′-Bromo-5′-deoxyguanosine and 5′-Chloro-5′-deoxyguanosine. Monoclinic crystals of **IIa**

DOI: 10.1021/acs.cgd.8b01162
Cryst. Growth Des. 2018, 18, 6995−7005

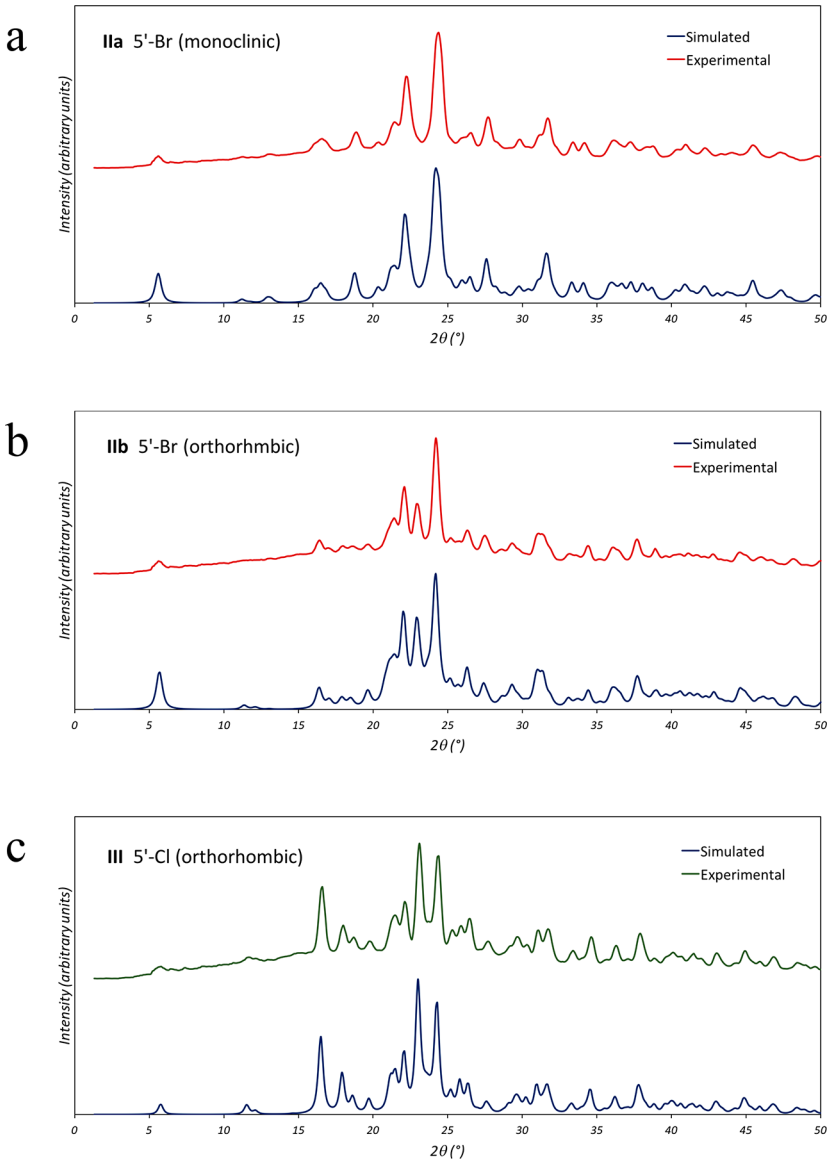

Figure 5. Qualitative comparison of experimental and calculated powder diffraction patterns for (a) **IIa**, (b) **IIb**, and (c) **III**. There are no spurious peaks in the experimental patterns, indicating that each batch was free of contamination by other polymorphs. For ease of comparison, simulated line widths were broadened to approximate experimental data.

are isostructural with **Ia** of PTGB (space group $P2_1$) while the orthorhombic form, **IIb**, is isostructural with **III** (space group $P2_12_12_1$). Some crystals of **IIa** were nonmerohedric twins by a twofold rotation about [001], but no twinning in **IIb** or **III** was detected.

*3.1.1. Molecular Geometry and Conformations in **IIa**, **IIb**, and **III**.* In spite of the symmetry differences, molecular conformations (Figures 1, 2, S2) and hydrogen-bonding patterns (Figure 3) in each of these crystal forms are essentially the same. Individual bond lengths and angles in **IIa**, **IIb**, and **III** are unremarkable. The following description is based on **IIa**, but except where stated otherwise, holds for each crystal structure. The overall geometry of the molecules is determined by the puckering of the deoxyribose ring, the torsion angle about the glycosidic bond, N9-C1′, which orients the flat purine ring system relative to the deoxyribose ring, and torsion about the C4′-C5′ bond, which orients the 5′-halo substituent relative to the deoxyribose ring. The deoxyribose ring has an envelope-type configuration, with atom C4′ as the "flap". Variation in ring puckering is negligible (Figure 2). Conformation defining parameters for **IIa**, **IIb**, and **III** are summarized in Table 2.

*3.1.2. Supramolecular Interactions in **IIa**, **IIb**, and **III**.* There are two main hydrogen-bonding motifs. An $R^1_2(6)$ motif involves a hydrogen of the exocyclic amine group, the NH of the six-membered ring, and the carbonyl oxygen (as a bifurcated acceptor) of a 2_1 screw-related molecule (Figure 3a). In addition, the hydroxyl groups of deoxyribose ring act as donors to the purine of an adjacent (diagonally in the *ab*-plane) molecule to form $R^2_2(10)$ rings (Figure 3b). As with **Ia** in PTGB, hydrogen bonds sandwich the molecules into double layers with the purine groups in the middle and exposed halogen atoms at the double-layer surfaces, but there are no $\pi-\pi$ interactions between adjacent purines. Hydrogen-bond parameters for **IIa**, **IIb**, and **III** are given in Table S1. It is the relative orientation of the double layers that defines the difference between the monoclinic and orthorhombic forms. In **IIa**, adjacent double layers stack along the *c*-direction purely

DOI: 10.1021/acs.cgd.8b01162
Cryst. Growth Des. 2018, 18, 6995−7005

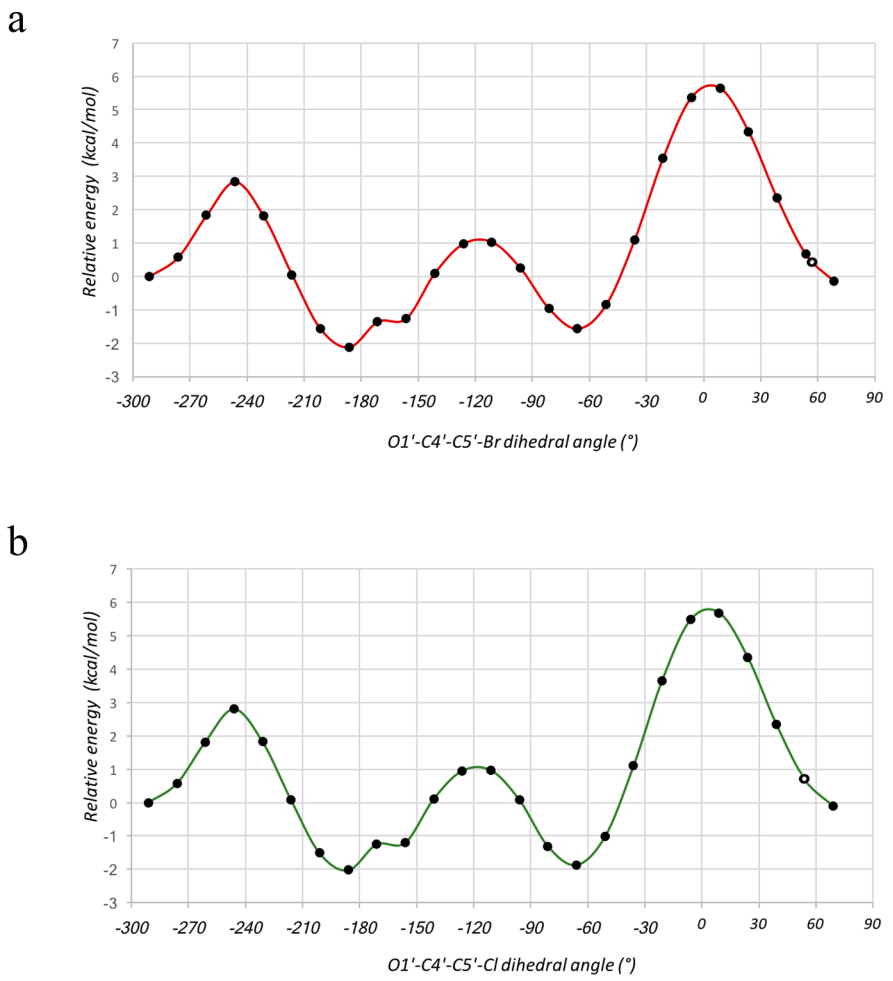

Figure 6. Isolated-molecule conformational energies for torsion (O1′−C4′−C5′−X) of the halogen atom relative to the deoxyribose group in (a) **II**, X = Br; (b) **III**, X = Cl. The starting points correspond to the local minima for the torsion angles after geometry optimization. Subsequent points correspond to optimized geometries after each increment of the torsion angle. Observed torsions from the crystal structures are indicated by open circles.

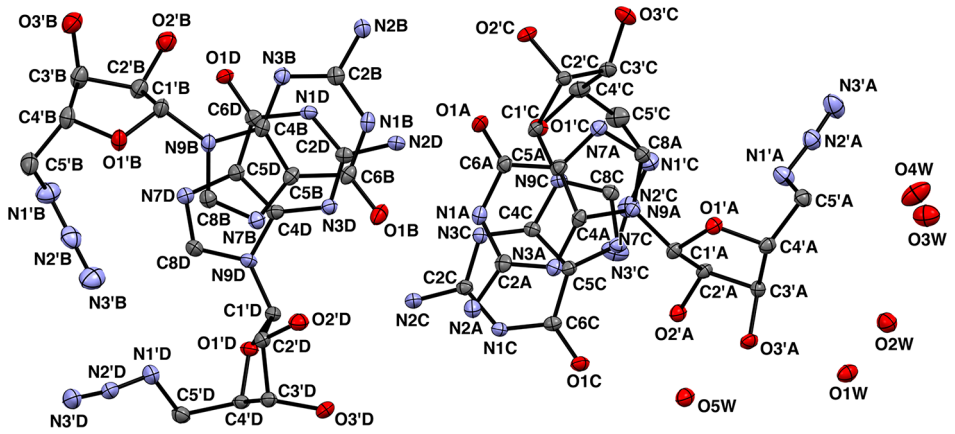

Figure 7. Ellipsoid plot (50% probability) of the asymmetric unit of **IV**. Hydrogen atoms are omitted to enhance clarity.

by the lattice translation. In **IIb**, however, alternate double layers are rotated 180° by virtue of the 2_1 screw axis along *c*, thereby doubling the repeat distance and forcing the β angle to 90° (Figures 4, S3). Indeed, the unit cell parameters for **IIa**, **IIb**, and **III** given in Table 1 are clearly related: transformation from the $P2_1$ cell metrics to those of the $P2_12_12_1$ cell amounts to fixing all cell angles to 90°, switching *a* and *b*, and doubling *c*, i.e., setting $a' = b$, $b' = a$, $c' = -2c$ (the sign change is required to preserve a right-handed system, and hence chirality). The relationship between adjacent double layers in **IIb** and **III**, i.e., 180° rotation about [001], is the same as the twin operation seen for some crystals of **IIa** (see section 3.4, below).

3.2. Powder Diffraction of IIa, IIb, and III. Although a few of the **IIa** crystals were non-merohedric twins, all single

DOI: 10.1021/acs.cgd.8b01162
Cryst. Growth Des. 2018, 18, 6995−7005

Table 3. Conformation-Defining Torsion Angles and Deoxyribose Ring Puckering Parameters for the Four Molecules in IV[a]

	Ic-A	Ic-B	IVa	IVb	IVc	IVd
C4−N9−C1′−O1′ (deg)	−154.1(7)	−76.2(9)	−153.1(3)	−149.2(3)	−75.5(4)	−140.4(3)
C8−N9−C1′−O1′ (deg)	38.2(11)	100.3(9)	34.8(4)	29.4(5)	95.8(4)	42.9(5)
O1′−C4′−C5′−X[b] (deg)	175.0(5)	−55.3(8)	−70.3(3)	−68.8(4)	−66.0(4)	−62.5(4)
C3′−C4′−C5′−X[b] (deg)	−66.8(8)	66.2(2)	49.3(4)	51.8(4)	52.9(4)	56.9(4)
C4′−C5′−N1′−N2′ (deg)			−175.3(3)	103.7(4)	90.6(4)	−147.2(3)
Cremer-Pople Q (Å)	0.405(9)	0.397(9)	0.386(3)	0.355(4)	0.344(4)	0.404(4)
Cremer-Pople Φ (deg)	83.6(11)	268.2912)	78.9(5)	54.3(6)	261.0(5)	82.6(5)

[a]For comparison, parameters for **Ic** from PTGB[5] are included. [b]**Ic**: X = iodine; **IV**: X = atom N1′ of the azide group.

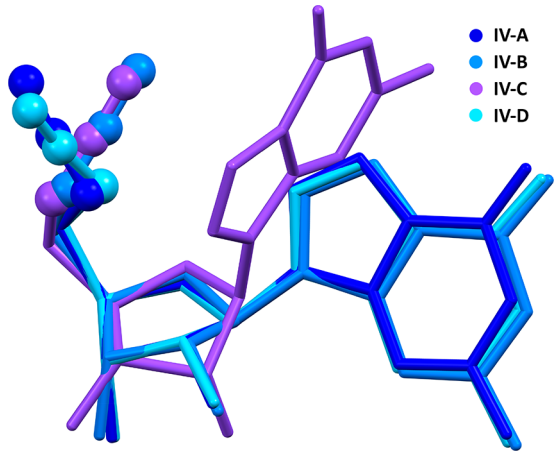

Figure 8. An overlay of the four crystallographically independent 5′-azido-5′-deoxyguanosines from a least-squares fit of the deoxyribose-ring atoms from the crystal structure of **IV**. Azide nitrogen atoms are drawn as balls for emphasis. Overlap of molecules **A** and **D** is close throughout. Molecule **B** is similar apart from torsion of the azide group. Molecule **C** has different puckering of its deoxyribose ring and torsion of the purine group, though its azide orientation is similar to that of **B**. An overlay based on a fit of the purine atoms is given in the Supporting Information (Figure S4).

and twinned specimens examined appeared to be phase pure. Comparison of powder diffraction patterns of separately pulverized batches of **IIa**, **IIb**, and **III** (Figure 5) compared to powder patterns calculated from the single-crystal structures show no evidence of contamination by even trace amounts of other polymorphs in any of the batches. A somewhat surprising result for **IIa** and **IIb** considering that the twin law for the few **IIa** twinned crystals observed is the same as the symmetry operation that relates alternate double layers in **IIb**.

3.3. Computational Modeling of II and III. Bond lengths and angles for the geometry optimized structures of **IIb** and **III** correspond well to the crystal structures. The overall conformations, however, differ to the extent that RMSD values between crystal structures and optimized geometries for **IIb** and **III** are 1.170 and 1.156 Å, respectively. Puckering of the deoxyribose rings changes such that the flap atom, C4′, flips to the other side of the mean plane through atoms O1′−C1′−C2′−C3′. The orientation of the flat purine ring relative to the deoxyribose ring defined by the torsion C4−N9−C1′−O1′ changes from −153.3(7)° to −116.34° in **IIa** and −153.4(4)° to −116.18° in **III**. Finally, the dihedral angle formed by O1′−C4′−C5′−X, while remaining *gauche*, expands in both **IIb** and **III**, from 58.3(7)° to 68.65° and 54.6(4)° to 69.03°, respectively. Changes in puckering and relaxation of the torsion angles in the optimized structures can be attributed to the condensed nature of the crystal packed structures in contrast with the calculated gas-phase structures. Results from the dihedral scans indicate that the *gauche* halogen atom conformations exhibited by the crystal structures are not the global minima on the potential energy surface (Figure 6). Rather, there exist *anti* conformations for both **IIb** and **III**, which sit ∼2.0 kcal/mol lower in energy (electronic energy without zero point or thermodynamic corrections applied) than the *gauche* conformers, similar to **I** in PTGB.[5]

3.4. Comparison of II, III, and the 5′-Iodo Analogue, Ia. Although superficially similar, there are clear differences between how planes of halogen atoms in the double layers interdigitate. In the monoclinic form, stacked double layers are identical by translation, whereas in the orthorhombic form they are rotated by 180° (Figures 4, S3 for **IIa** and **IIb**). That polymorphic forms and non-merohedric twinning were only found for the 5′-Br compound suggests that the absence of either a monoclinic polymorph of **III** or an orthorhombic form of **I** might be due to the effect of halogen atom size and the strength of halogen−halogen atom interactions. Attempts to find a straightforward thermodynamic explanation for this phenomenon via computational modeling were unsuccessful. A plausible explanation, however, might be that it is due to the kinetics of crystal growth, influenced by the steric compatibility of interacting planes of halogen atoms on adjacent double layers. In other words, the 5′-halogen atom size and mode of contact determine which forms are stable, i.e., 5′-I (**Ia**, monoclinic only), 5′-Cl (**III**, orthorhombic only), or 5′-Br (**IIa**, monoclinic and **IIb**, orthorhombic). Since the relationship between adjacent double layers in **IIb** and twinning in **IIa** are both twofold rotation about [001], it is perhaps surprising that each batch of the 5′-Br compound appeared to be phase pure.

3.5. Structure of 5′-Azido-5′-deoxyguanosine Hydrate, IV. The crystal structure of **IV** proved to be considerably more complicated than any of the 5′-halo derivatives. The asymmetric unit contains four molecules (**A**, **B**, **C**, **D**) of the 5′-azido-5′-deoxyguanosine and five full-occupancy well-defined water molecules (Figure 7).

3.5.1. Molecular Geometry and Conformation in IV. Bond lengths and angles are all normal. Molecular geometry can be described by the same torsion angles and ring puckering parameters as the 5′-halo analogues with the addition of torsion about the C5′−N1′ bond, which orients the N_3 group relative to the deoxyribose ring (Table 3). Unlike the 5′-halo analogues, the four main molecules adopt a range of conformations. Molecules **A** and **D** have similar geometry, while **B** differs from **A** and **D** primarily by torsion of the azide. Molecule **C**, however, is different in almost all respects, especially puckering of the deoxyribose ring. This, in combination with the glycosidic bond torsion, dramatically changes the position of its purine group relative to the deoxyribose ring (Table 3, Figures 8, S4).

DOI: 10.1021/acs.cgd.8b01162
Cryst. Growth Des. 2018, 18, 6995−7005

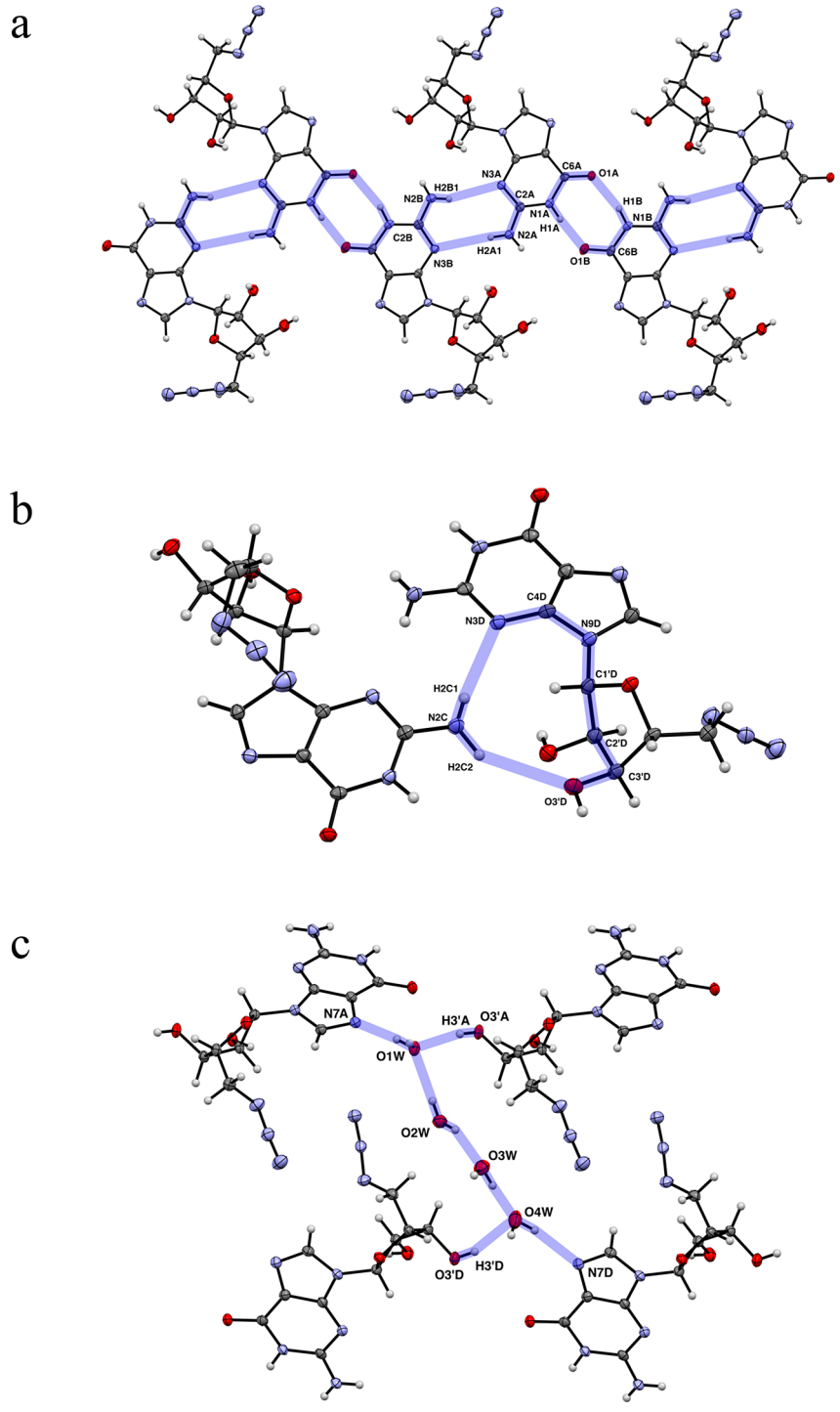

Figure 9. Major hydrogen-bond motifs in **IV**, highlighted by semitransparent blue lines. (a) Pairs of $R^2_2(8)$ rings link molecules **A** and **B** into ribbons parallel to (−1, 3, 0). Similar ribbons form between molecules **C** and **D** (Figure S5a). (b) An $R^2_2(10)$ ring joins the exocyclic amine of **C** to the purine and deoxyribose rings of **D**. (c) A chain of four water molecules joins pairs of **A** molecules (top) to pairs of **D** molecules (bottom).

*3.5.2. Pairing of Molecules by π−π Interactions in **IV**.* Within the asymmetric unit the purine groups of **A** and **C** stack so as to place the 6-membered ring of **A** over the 5-membered ring of **C**, with a distance between their respective centroids of 3.309(4) Å. The dihedral angle between the planes of purines in **A** and **C** is 4.0(1)°. Stacking of the **B** and **D** molecules places atom C5B almost directly over the 6-membered ring of **D** such that the distance between its centroid and C5B is 3.330(4) Å. The dihedral between purines in **B** and **D** is 9.17(11)°. These overlaps are readily apparent in the ellipsoid plot of the asymmetric unit (Figure 7).

*3.5.3. Hydrogen Bonding in **IV**.* The primary intermolecular motifs involving just main molecules **A**, **B**, **C**, **D** are extended ribbons. An $R^2_2(8)$ motif joins the 6-membered purine rings of **A** and **B** in the same asymmetric unit by their NH (donor) and carbonyl oxygen (acceptor) atoms. A different type of $R^2_2(8)$ ring pairs the **A** molecule exocyclic amine (donor) and 6-membered ring nitrogen (acceptor) with their counterparts

DOI: 10.1021/acs.cgd.8b01162
Cryst. Growth Des. 2018, 18, 6995−7005

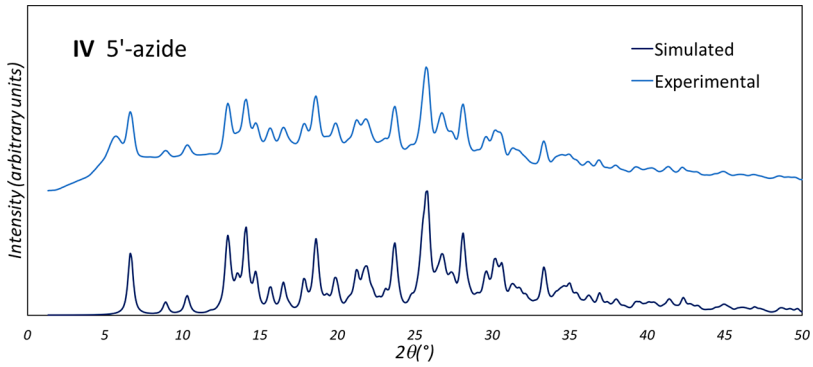

Figure 10. Qualitative comparison of experimental and calculated powder diffraction patterns for **IV**. All peaks present in the simulated plot match well to experimental peaks. Only one broad peak at low diffraction angle in the experimental plot has no counterpart in the simulation. The cause of this broad feature remains unknown, but is likely due to ground sample that had dried and lost its crystallinity.

on a translation related **B**$(x, y, z-1)$. These motifs repeat to form ribbons parallel to $(-1, 3, 0)$ that propagate along c (Figure 9a). Similar constructs exist between molecules **C** and **D**, also forming ribbons parallel to $(-1, 3, 0)$ that extend along c (Figure S5a). Finally, an $R^2_2(10)$ ring links the exocyclic amine of **C** with the 6-membered ring nitrogen and O3′ (acceptors) of **D** in the same asymmetric unit (Figure 9b). The presence of five water molecules complicates the description of hydrogen bonding. Four of the water molecules (W1, W2, W3, W4) form a chain linking translation-related N7A$(x, y, z-1)$ and 2_1 screw-related N7D$(1-x, y-0.5, 2-z)$. This water chain is sandwiched between the azide and deoxyribose of **A** (same asymmetric unit) and their counterparts on a screw-related **D**$(1-x, y-0.5, 1-z)$ (Figure 9c). Water W5, which is isolated from the other waters in a pocket, hydrogen bonds as a donor to carbonyl O1C (same asymmetric unit) and a translation-related hydroxyl O2′C$(x, y, z-1)$, and as an acceptor of one hydrogen from the exocyclic amine of **D** in the same asymmetric unit (Figure S5b). Hydrogen-bond parameters in **IV** are given in Table S2.

3.6. Powder Diffraction of IV. All single crystals of **IV** examined in detail indexed to give the same unit cell as the hydrate crystal used for structure determination. Comparison of powder diffraction patterns for a pulverized batch of crystals and a pattern calculated from the single-crystal structure showed good agreement between peak positions except for a single broad feature at about $2\theta = 5.5°$ in the experimental plot that is absent in the simulation (Figure 10). The cause of this extra broad peak remains unknown but it could simply be due to material that had wholly or partially dried. The parent compound, guanosine, is known to undergo a reversible transition between a dihydrate and an anhydrous form depending on the relative humidity.[49] All other peaks match well to the simulation, so there does not appear to be any other *crystalline* phase present.

3.7. Computational Modeling of IV. The four crystallographically independent molecules **A**, **B**, **C**, and **D**, were subjected to computational analysis to assess the relative stability of each conformation. Starting from the crystallographic coordinates, the structures were optimized into their respective local-energy minima (see section 2.5 for details), giving idealized gas-phase conformations for each: $\mathbf{A}_g$, $\mathbf{B}_g$, $\mathbf{C}_g$, and $\mathbf{D}_g$. These were then solvated using the SMD continuum solvation model[48] and further energy optimized. The results are condensed into Table 4. From the gas-phase calculations, conformations $\mathbf{A}_g$ and $\mathbf{D}_g$ are essentially equivalent. The most stable conformer is $\mathbf{C}_g$, whose parent conformation (**C**) is the visual odd-man-out in Figure 8. The highest energy conformer is $\mathbf{B}_g$, whose parent in the crystal (**B**) shares a similar guanosine conformation with **A** and **D**, but a different torsion of the azide group. Solvated model conformations, $\mathbf{A}_w$, $\mathbf{B}_w$, $\mathbf{C}_w$, and $\mathbf{D}_w$ are perhaps more instructive for their crystal growth implications. Here, the most stable solvated conformation is $\mathbf{B}_w$, so it is presumably the closest to the dominant conformation in aqueous solution. Not surprisingly, equivalent conformers $\mathbf{A}_w$ and $\mathbf{D}_w$ are still equivalent in the solvated model.

Table 4. Energies of Geometry-Optimized Conformers from IV Relative to the Lowest Energy (Computed) Conformer[a]

(a) Relative gas-phase energies (kcal/mol) for **IV** molecules with respect to lowest energy conformer

	ΔE_0	ΔH_0	ΔH_{298}	ΔG_{298}
$\mathbf{A}_g$	2.72	2.15	2.52	1.83
$\mathbf{B}_g$	3.17	2.69	3.03	2.58
$\mathbf{C}_g$	0.00	0.00	0.00	0.00
$\mathbf{D}_g$	2.72	2.15	2.52	1.83

(b) Relative solvated energies (kcal/mol) for **IV** molecules with respect to lowest energy conformer

	ΔE_0	ΔH_0	ΔH_{298}	ΔG_{298}
$\mathbf{A}_w$	1.78	1.66	1.75	1.33
$\mathbf{B}_w$	0.00	0.00	0.00	0.00
$\mathbf{C}_w$	0.71	0.96	0.87	1.62
$\mathbf{D}_w$	1.78	1.66	1.75	1.32

[a]Optimization and frequency analysis for (a) gas phase and (b) solvated (SMD model) conformers performed at the B3LYP/6-311+G** level of theory.

3.8. Comparison of IV and the Solvate of the 5′-Iodo Analogue, I. The hydrate structure of **IV** shares many similarities with **Ic**, the water/methanol solvate of **I** in PTGB,[5] which has two main molecules in its asymmetric unit. In spite of the more complicated asymmetric unit in **IV** ($Z' = 4$, space group $P2_1$) vs **Ic** ($Z' = 2$, space group $P2_12_12_1$), the a axes of **IV** and **Ic** are similar (9.2318(2) Å vs 9.2724(2) Å, respectively), as are the c axis of **IV** and the b axis of **Ic** (10.8838(2) Å and 10.5929(3) Å, respectively). A much greater difference exists between the b axis of **IV** (27.0190(2) Å) and the c axis of **Ic** (32.2592(8) Å), but the solvent content is higher and less well-defined in **Ic** than in **IV**. In terms of molecular geometry, molecule **IV-C** is similar to one of the two main molecules, **Ic-B**, in the asymmetric unit of **Ic** (Figure S6a), whereas molecules **A**, **B**, and **D** of **IV** are similar to **Ic-A**, the

DOI: 10.1021/acs.cgd.8b01162
Cryst. Growth Des. 2018, 18, 6995−7005

other main molecule in **Ic** (Figure S6b). The different types of hydrogen-bonding motifs in **IV** (two different $R^2_2(8)$, and an $R^2_2(10)$ ring) are also present in **Ic**, but none of the motifs that are preserved in all the nonsolvated 5′-halo structures are found in **IV** (or **Ic**). Similar $\pi-\pi$ overlap of purine groups is also present in **Ic**.

4. SUMMARY

The unusual conformational polymorphism in monoclinic hybrid crystals of 5′-iodo-5′-deoxyguanosine is not exhibited by either the 5′-Br or 5′-Cl analogues. The molecular conformation present in the minor polymorph of solvent-free 5′-I is absent in all solvent-free forms of crystalline 5′-Br and 5′-Cl-guanosine. Instead, only crystal forms related to the dominant 5′-I conformation, which consists of stacks of identical double layers, are found. The 5′-Br compound forms two polymorphs: a monoclinic structure that is isotypic to the dominant 5′-I polymorph, and an orthorhombic polymorph in which alternating double layers are rotated by 180° about [001]. Some of the 5′-Br monoclinic crystals were twinned, wherein the twin operation is also a 180° rotation about [001] of abutted twin components, entirely analogous to the relationship between double layers in the orthorhombic polymorph. For the 5′-Cl compound, only the orthorhombic isotype was observed. Attempts to find a simple thermodynamic means to predict preference for monoclinic $P2_1$ versus orthorhombic $P2_12_12_1$ structure types as a function of 5′-halogen substituent via computational modeling were unsuccessful. As with the preference for **Ia** over **Ib** in PTGB, the kinetics of crystal growth, influenced by the steric compatibility of interacting planes of halogen atoms on adjacent double layers might be the decisive factor.

Unlike the 5′-halo derivatives, the pseudohalide 5′-azido compound **IV** only crystallized to give a hydrate structure, with many of the same features as the water/methanol solvate **Ic**. In spite of the similarities, perhaps the most striking difference between crystals of **IV** and **Ic** is the propensity for growth of each particular crystal form. Crystals of the hydrated structure of **IV** described here were abundant, and were the *only* crystal form of 5′-azido-5′-deoxyguanosine isolated, despite many crystallization trials and many solvent combinations. **Ic** on the other hand was only encountered once, in an early (actually the *first*) batch of crystals of **I** encountered in PTGB.[5]

ASSOCIATED CONTENT

Supporting Information

The Supporting Information is available free of charge on the ACS Publications website at DOI: 10.1021/acs.cgd.8b01162.

> Hydrogen bonding in **IIa**, **IIb**, and **III**. Hydrogen bonding in **IV**. Photographs of typical crystals of **IIa**, **IIb**, **III**, **IV**. Ellipsoid plot (50% probability) of **IIb**. Alternation of double layers in **IIa** and **IIb**. Overlay of four crystallographically independent 5′-azido-5′-deoxyguanosines in **IV**. Some hydrogen-bond motifs in **IV**. Overlays of selected molecules **IV** and **Ic**. (PDF)

Accession Codes

CCDC 1859457−1859460 contain the supplementary crystallographic data for this paper. These data can be obtained free of charge via www.ccdc.cam.ac.uk/data_request/cif, or by emailing data_request@ccdc.cam.ac.uk, or by contacting The Cambridge Crystallographic Data Centre, 12 Union Road, Cambridge CB2 1EZ, UK; fax: +44 1223 336033.

AUTHOR INFORMATION

Corresponding Author

*E-mail: s.parkin@uky.edu.

ORCID

Sean R. Parkin: 0000-0001-5777-3918

Edward J. Behrman: 0000-0002-8797-6625

Author Contributions

Synthesis and crystallization was carried out by E.J.B. Crystallographic analyses were performed by S.R.P. Computational work was conducted by W.H.C. and J.P.F., while guided by C.M.H. The manuscript contains contributions from all authors and all authors have read and approved the final version of the manuscript.

Notes

The authors declare no competing financial interest.

ACKNOWLEDGMENTS

Crystallographic work was made possible by the National Science Foundation (NSF) MRI program, grants CHE-0319176 and CHE-1625732 to S.R.P. C.M.H. acknowledges financial support from the NSF (CHE-1609889) as well as generous allocations of computational resources from the Ohio Supercomputer Center.

REFERENCES

(1) Brear, P.; Freeman, G. R.; Shankey, M. C.; Trmcĭć, M.; Hodgson, D. R. W. Aqueous methods for the preparation of 5′-substituted guanosine derivatives. *Chem. Commun.* **2009**, 4980−4981.

(2) Zhang, B.; Cui, Z.; Sun, L. Synthesis of 5′-Deoxy-5′-thioguanosine-5′-monophosphorothioate and Its Incorporation into RNA 5′-Termini. *Org. Lett.* **2001**, *3*, 275−278.

(3) Fiammengo, R.; Musílek, K.; Jäschke, A. Efficient Preparation of Organic Substrate−RNA Conjugates via in Vitro Transcription. *J. Am. Chem. Soc.* **2005**, *127*, 9271−9276.

(4) Williamson, D.; Cann, M. J.; Hodgson, D. R. W. Synthesis of 5′-amino-5′-deoxyguanosine-5′-N-phosphoramidate and its enzymatic incorporation at the 5′-termini of RNA molecules. *Chem. Commun.* **2007**, 5096−5098.

(5) Parkin, S. R.; Thorley, K. J.; Gagnon, K. J.; Behrman, E. J. Epitaxially Intergrown Conformational Polymorphs and a Mixed Water/Methanol Solvate of 5′-Deoxy-5′-iodoguanosine. *Cryst. Growth Des.* **2016**, *16*, 6343−6352.

(6) Bernstein, J. *Polymorphism in Molecular Crystals*; Oxford University Press: Oxford, UK, 2002.

(7) Parkin, S.; Hope, H. Uric Acid Dihydrate Revisited. *Acta Crystallogr., Sect. B: Struct. Sci.* **1998**, *54*, 339−344.

(8) Jahangiri, A.; Fleckhaus, A.; Lidin, S.; Strand, D. Allotwinning in a molecular crystal: (1R,3S)-dimethyl 2-oxocyclohexane-1, 3-dicarboxylate. *Acta Crystallogr., Sect. B: Struct. Sci., Cryst. Eng. Mater.* **2013**, *69*, 509−513.

(9) Kautny, P.; Schwartz, T.; Stöger, B.; Fröhlich, J. An unusual case of OD-allotwinning: 9,9′-(2,5-dibromo-1,4-phenylene)bis[9H-carbazole]. *Acta Crystallogr., Sect. B: Struct. Sci., Cryst. Eng. Mater.* **2017**, *73*, 65−73.

(10) Nespolo, M.; Ferraris, G.; Takeda, H. Identification of two allotwins of mica polytypes in reciprocal space through the minimal rhombus unit. *Acta Crystallogr., Sect. B: Struct. Sci.* **2000**, *56*, 639−647.

(11) Nespolo, M.; Kogure, T.; Ferraris, G. Allotwinning: oriented crystal association of polytypes − some warnings on consequences. *Z. Kristallogr. - Cryst. Mater.* **1999**, *214*, 5−8.

(12) Kóšiová, I.; Rosenberg, I. Synthesis of nucleoside 5′-S-methylphosphonates and related compounds. *Nucleic Acids Symp. Ser.* **2008**, *52* (52), 569−570.

DOI: 10.1021/acs.cgd.8b01162
Cryst. Growth Des. 2018, 18, 6995−7005

(13) Perchyonok, V. T. Black Light Induced Radical Cyclization Approach to Cyclonucleosides: An Independent Approach. *Lett. Org. Chem.* **2011**, *8*, 337−340.
(14) Tomasz, J.; Vaghefi, M. M.; Ratsep, P. C.; Willis, R. C.; Robins, R. K. Nucleoside imidodiphosphates synthesis and biological activities. *Nucleic Acids Res.* **1988**, *16*, 8645−8664 Note that the designation of the compound in Table 1 is 6c, not 5c.
(15) Tsalmane, L. V.; Lidak, M. J. Synthesis of 5′-Deoxynucleoside-5′-thiosulfuric acids of the Purine Series. *Bioorg. Khim.* **1990**, *16*, 969−975.
(16) van Tilburg, E. W.; Künzel, J.; de Groote, M.; IJzerman, A. P. 2,5′-Disubstituted Adenosine Derivatives: Evaluation of Selectivity and Efficacy for the Adenosine A1, A2A, and A3 Receptor. *J. Med. Chem.* **2002**, *45*, 420−429.
(17) Jamison, M. T.; Boddy, C. N.; Molinsky, T. F. Salvadenosine, a 5′-Deoxy-5′-(methylthio) Nucleoside from the Bahamian Tunicate Didemnum sp. *J. Org. Chem.* **2014**, *79*, 9992−9997.
(18) Jahn, W. Synthese 5′-substituierter Adenosinderivate. *Chem. Ber.* **1965**, *98*, 1705−1708.
(19) Dean, D. K. An Improved Synthesis Of 5′-Amino-5′-Deoxyguanosine. *Synth. Commun.* **2002**, *32*, 1517−1521.
(20) Paredes, E.; Das, S. R. Click Chemistry for Rapid Labeling and Ligation of RNA. *ChemBioChem* **2011**, *12*, 125−131.
(21) Paredes, E.; Evans, M.; Das, S. R. RNA labeling, conjugation and ligation. *Methods* **2011**, *54*, 251−259.
(22) Warminsky, M.; Kowalska, J.; Jemielty, J. Synthesis of RNA 5′-Azides from 2′-O-Pivaloyloxymethyl-Protected RNAs and Their Reactivity in Azide−Alkyne Cycloaddition Reactions. *Org. Lett.* **2017**, *19*, 3624−3627.
(23) Appel, R. Tertiary Phosphane/Tetrachloromethane, a Versatile Reagent for Chlorination, Dehydration, and P-N Linkage. *Angew. Chem., Int. Ed. Engl.* **1975**, *14*, 801−811.
(24) Tsuji, T.; Takenaka, K. Facile 5′-Halogenation of Unprotected Nucleosides. *Nucleosides, Nucleotides Nucleic Acids* **1987**, *6*, 575−580.
(25) Finkelstein, H. Darstellung organischer Jodide aus den entsprechenden Bromiden und Chloriden. *Ber. Dtsch. Chem. Ges.* **1910**, *43*, 1528−1532.
(26) McGee, D. P. C.; Martin, J. C. Acyclic nucleoside analogues: methods for the preparation of 2′,3′-secoguanosine, 5′-deoxy-2′,3′-secoguanosine, and (R,S)-9-[1-(2-hydroxyethoxy)-2-hydroxyethyl]-guanine. *Can. J. Chem.* **1986**, *64*, 1885−1889.
(27) Parker, A. J. Solvation of ions. Part II. Dipolar aprotic solvents as media for nucleophilic substitution reactions at a saturated carbon atom. *J. Chem. Soc.* **1961**, 1328−1337.
(28) Hope, H. X-Ray Crystallography: A Fast, First-Resort Analytical Tool. *Prog. Inorg. Chem.* **2007**, *41*, 1−19.
(29) Parkin, S.; Hope, H. Macromolecular Cryocrystallography: Cooling, Mounting, Storage and Transportation of Crystals. *J. Appl. Crystallogr.* **1998**, *31*, 945−953.
(30) *APEX2; Programs for X-Ray Data Collection and Reduction*; Bruker-AXS Inc.: Madison, WI, USA, 2006.
(31) *APEX3; Programs for X-Ray Data Collection and Reduction*; Bruker-AXS Inc.: Madison, WI, USA, 2016.
(32) Krause, L.; Herbst-Irmer, R.; Sheldrick, G. M.; Stalke, D. Comparison of silver and molybdenum microfocus X-ray sources for single-crystal structure determination. *J. Appl. Crystallogr.* **2015**, *48*, 3−10.
(33) Parkin, S.; Moezzi, B.; Hope, H. XABS2: an empirical absorption correction program. *J. Appl. Crystallogr.* **1995**, *28*, 53−56.
(34) Sheldrick, G. M. SHELXT − Integrated space-group and crystal-structure determination. *Acta Crystallogr., Sect. A: Found. Adv.* **2015**, *71*, 3−8.
(35) Sheldrick, G. M. Crystal structure refinement with SHELXL. *Acta Crystallogr., Sect. C: Struct. Chem.* **2015**, *71*, 3−8.
(36) Spek, A. L. PLATON SQUEEZE: a tool for the calculation of the disordered solvent contribution to the calculated structure factors. *Acta Crystallogr., Sect. C: Struct. Chem.* **2015**, *71*, 9−18.
(37) Spek, A. L. Single-crystal structure validation with the program PLATON. *J. Appl. Crystallogr.* **2003**, *36*, 7−13.
(38) Parkin, S. Expansion of scalar validation criteria to three dimensions: an R-tensor. *Acta Crystallogr., Sect. A: Found. Crystallogr.* **2000**, *56*, 157−162.
(39) *checkCIF*; http://checkcif.iucr.org.
(40) Macrae, C. F.; Edgington, P. R.; McCabe, P.; Pidcock, E.; Shields, G. P.; Taylor, R.; Towler, M.; van de Streek, J. Mercury: visualization and analysis of crystal structures. *J. Appl. Crystallogr.* **2006**, *39*, 453−457.
(41) Frisch, M. J.; Trucks, G. W.; Schlegel, H. B.; Scuseria, G. E.; Robb, M. A.; Cheeseman, J. R.; Scalmani, G.; Barone, V.; Petersson, G. A.; Nakatsuji, H.; Li, X.; Caricato, M.; Marenich, A. V.; Bloino, J.; Janesko, B. G.; Gomperts, R.; Mennucci, B.; Hratchian, H. P.; Ortiz, J. V.; Izmaylov, A. F.; Sonnenberg, J. L.; Williams-Young, D.; Ding, F.; Lipparini, F.; Egidi, F.; Goings, J.; Peng, B.; Petrone, A.; Henderson, T.; Ranasinghe, D.; Zakrzewski, V. G.; Gao, J.; Rega, N.; Zheng, G.; Liang, W.; Hada, M.; Ehara, M.; Toyota, K.; Fukuda, R.; Hasegawa, J.; Ishida, M.; Nakajima, T.; Honda, Y.; Kitao, O.; Nakai, H.; Vreven, T.; Throssell, K.; Montgomery, J. A., Jr.; Peralta, J. E.; Ogliaro, F.; Bearpark, M. J.; Heyd, J. J.; Brothers, E. N.; Kudin, K. N.; Staroverov, V. N.; Keith, T. A.; Kobayashi, R.; Normand, J.; Raghavachari, K.; Rendell, A. P.; Burant, J. C.; Iyengar, S. S.; Tomasi, J.; Cossi, M.; Millam, J. M.; Klene, M.; Adamo, C.; Cammi, R.; Ochterski, J. W.; Martin, R. L.; Morokuma, K.; Farkas, O.; Foresman, J. B.; Fox, D. J. *Gaussian 16*, Revision A.03; Gaussian, Inc., Wallingford, CT, 2016.
(42) Becke, A. D. Density-functional exchange-energy approximation with correct asymptotic behavior. *Phys. Rev. A: At., Mol., Opt. Phys.* **1988**, *38*, 3098−3100.
(43) Lee, C.; Yang, W.; Parr, R. G. Development of the Colle-Salvetti correlation-energy formula into a functional of the electron density. *Phys. Rev. B: Condens. Matter Mater. Phys.* **1988**, *37*, 785−789.
(44) Becke, A. D. A new mixing of Hartree−Fock and local density-functional theories. *J. Chem. Phys.* **1993**, *98*, 1372−1377.
(45) Hehre, W. J.; Radom, L.; Schleyer, P. v. R.; Pople, J. A. *Ab Initio Molecular Orbital Theory*; John Wiley & Sons: New York, 1986.
(46) Pettersen, E. F.; Goddard, T. D.; Huang, C. C.; Couch, G. S.; Greenblatt, D. M.; Meng, E. C.; Ferrin, T. E. UCSF Chimera–a visualization system for exploratory research and analysis. *J. Comput. Chem.* **2004**, *25*, 1605−1612.
(47) Dennington, R.; Keith, T. A.; Millam, J. M. *GaussView*, v 6.0.16; Semichem Inc.: Shawnee Mission, KS, 2016.
(48) Marenich, A. V.; Cramer, C. J.; Truhlar, D. G. Universal Solvation Model Based on Solute Electron Density and on a Continuum Model of the Solvent Defined by the Bulk Dielectric Constant and Atomic Surface Tensions. *J. Phys. Chem. B* **2009**, *113*, 6378−6396.
(49) Sugawara, Y.; Iimura, Y.; Iwasaki, H.; Urabe, H.; Saito, H. Reversible Crystal Transition of Guanosine between the Dihydrate and Anhydrous States Coupled with Adsorption-Desorption Process. *J. Biomol. Struct. Dyn.* **1994**, *11*, 721−729.

DOI: 10.1021/acs.cgd.8b01162
Cryst. Growth Des. 2018, 18, 6995−7005